

# A Universal Temperature Profile for Galaxy Clusters

Chris Loken<sup>1</sup>, Michael L. Norman<sup>2</sup>, Erik Nelson<sup>2</sup>, Jack Burns<sup>3</sup>, Greg L. Bryan<sup>4</sup>, Patrick Motl<sup>3</sup>

## ABSTRACT

We investigate the predicted present-day temperature profiles of the hot, X-ray emitting gas in galaxy clusters for two cosmological models - a current best-guess  $\Lambda$ CDM model and standard cold dark matter (SCDM). Our numerically-simulated “catalogs” of clusters are derived from high-resolution ( $15 \text{ h}^{-1} \text{ kpc}$ ) simulations which make use of a sophisticated, Eulerian-based, Adaptive Mesh-Refinement (AMR) code that faithfully captures the shocks which are essential for correctly modelling cluster temperatures. We show that the temperature structure on Mpc-scales is highly complex and non-isothermal. However, the temperature profiles of the simulated  $\Lambda$ CDM and SCDM clusters are remarkably similar and drop-off as  $T \propto (1 + r/a_x)^{-\delta}$  where  $a_x \sim r_{vir}/1.5$  and  $\delta \sim 1.6$ . This decrease is in good agreement with the observational results of Markevitch et al. (1998) but diverges, primarily in the innermost regions, from their fit which assumes a polytropic equation of state. Our result is also in good agreement with a recent sample of clusters observed by *BeppoSAX* though there is some indication of missing physics at small radii ( $r < 0.2 r_{vir}$ ). We discuss the interpretation of our results and make predictions for new x-ray observations that will extend to larger radii than previously possible. Finally, we show that, for  $r > 0.2 r_{vir}$ , our universal temperature profile is consistent with our most recent simulations which include both radiative cooling and supernovae feedback.

*Subject headings:* cosmology:theory – galaxies:clusters:general – hydrodynamics – intergalactic medium – X-rays:galaxies

## 1. Introduction

X-ray based cluster mass determinations generally assume that morphologically-symmetric

(i.e. non-merging) clusters are isothermal. However, this accepted wisdom has recently been challenged by Markevitch et al. (1998; hereafter M98) who found evidence for decreasing temperature profiles in a sample of nearby hot clusters ( $> 3.5 \text{ keV}$ ) observed with ASCA. A subsample of 17 regular/symmetric clusters displayed remarkably similar temperature profiles (when normalized and scaled by the virial radius) consistent with  $T \propto [1 + (r/r_c)^2]^{-3\beta(\gamma-1)/2}$  where  $\gamma = 1.24^{+0.20}_{-0.12}$  and  $\beta = 2/3$ . The typical decrease is there-

---

<sup>1</sup>Canadian Institute for Theoretical Astrophysics, 60 St. George St., University of Toronto, Toronto, ON M5S 3H8

<sup>2</sup>Center for Astrophysics & Space Sciences, University of California, San Diego, CA

<sup>3</sup>Department of Astrophysical and Planetary Sciences, University of Colorado, Boulder, CO 80309

<sup>4</sup>University of Oxford, Astrophysics, Keble Road, Oxford, OX1 3RH

fore a factor of  $\sim 2$  in going from 1 to 6 core radii (or .09 to 0.5 virial radii). This result remains controversial as three subsequent studies of large samples of clusters concluded that the majority of cluster temperature profiles show little, or no, decrease with radius (Irwin, Bregman, & Evrard 1999; White 2000; Irwin & Bregman 2000). Most recently, De Grandi & Molendi (2002) have presented a composite temperature profile based on *BeppoSAX* data which exhibits an isothermal core and then decreases quickly. Here we present results derived from recent high-resolution numerical simulations and show that there appears to be a universal temperature profile which declines significantly even within half a virial radius of the cluster center. We also show that these simulated profiles are consistent with the most recent cluster observations except in the very innermost regions of a cluster ( $r < 0.2 r_{vir}$ ).

## 2. Simulations

The simulated clusters used in this work are part of an ongoing project to create extensive numerical “catalogs” of clusters. This catalog has already been used to investigate the effect of large-scale structure on weak gravitational lensing mass estimates (Metzler et al. 1999, 2001) and the role of “temperature bias” in Sunyaev-Zeldovich determinations of the Hubble constant (Lin, Norman, & Bryan 2001). The cluster simulation data are available on-line at the Simulated Cluster Archive: <http://sca.ncsa.uiuc.edu> (Norman et al. 1999).

The cosmological model adopted for the bulk of the simulations is a current “best-guess” flat universe with a cosmological constant ( $\Lambda$ CDM) and parameters:  $\Omega_0 = 0.3$ ,  $\Omega_b = 0.026$ ,  $\Omega_\Lambda = 0.7$ ,  $h = 0.7$  and  $\sigma_8 = 0.928$ . The 25 most-massive clusters in the  $256 h^{-1}$  Mpc volume have been fully analyzed and comprise the  $\Lambda$ CDM sample used in

this work. For comparison, a smaller sample of 10 SCDM clusters has been simulated in the same volume (and with the same random-seed for the initial fluctuations) with parameters:  $\Omega_0 = 1$ ,  $\Omega_b = 0.076$ ,  $h = 0.5$  and  $\sigma_8 = 0.6$

An initial low-resolution simulation was used to identify clusters in the  $256 h^{-1}$  Mpc volume and then high-resolution simulations were performed which evolved the entire volume but adaptively refined the region from which a specific cluster formed. The root, or level 0 (L0), grid covers the entire periodic domain with  $128^3$  cells. The Lagrangian volume of a given cluster is further refined with two levels of subgrids (L1 and L2), each with twice the spatial resolution and eight times the mass resolution of the previous one, in order to refine the initial conditions within this volume. An additional five levels of refinement are introduced adaptively and automatically within the L2 grid as the simulation progresses. The clusters form from particles on the L2 grid which have a mass of  $9 \times 10^9 h^{-1} M_\odot$ . The best spatial resolution is  $15.6 h^{-1} \text{kpc}$ .

The cosmological adaptive-mesh refinement (AMR) code used here is described in detail in Bryan (1999) and Norman & Bryan (1999). Briefly, this code solves the equations of hydrodynamics using the higher-order accurate piecewise parabolic method (PPM; Collela & Woodward 1984) and employs an adaptive particle-mesh algorithm (using second-order accurate TSC interpolation) for the dark matter particles. The Eulerian hydrodynamics algorithm exhibits several crucial characteristics including excellent shock-capturing (within 1-2 zones with correct entropy generation), and equal accuracy in high or low density regions (for the same zone size). The key component of the code is its use of structured adaptive mesh refinement (Berger & Collela 1989) in order to enhance resolution when and where needed.

Our code was tested as part of the Santa

Barbara cluster comparison project (Frenk et al. 1999) in which 12 groups simulated a Coma-like cluster using a variety of codes and resolutions. Our results (curves labeled “bryan”) are among the highest resolution results presented in that paper (central resolution of  $7.8h^{-1}$  kpc). We agree well with the highest resolution *AP<sup>3</sup>MSPH* results except that our central temperature is somewhat higher, and our radial temperature profiles continue to rise at small radii rather than flattening within 200 kpc. Frenk et al. (1999) note that this discrepancy is more or less present in all the grid-based codes but provide no explanation. To check whether this might be a result of numerical resolution or algorithms employed, we recomputed the Santa Barbara cluster with low, medium and high resolution initial conditions corresponding to  $64^3$ ,  $128^3$  and  $256^3$  particles/cells in the L0 grid, and L7 resolutions equal to 15.6, 7.8, and  $3.9h^{-1}$  kpc, respectively. Instead of PPM, we also tested the artificial viscosity, finite-difference algorithm for gas dynamics used in the ZEUS codes (Stone & Norman 1992). In all cases we found the temperature profile agreed with our result presented in Frenk et al. to within a few percent at all radii; i.e., our temperature profile has converged. Note also that there is excellent agreement between our results for the Santa Barbara cluster and those of a new, completely independent AMR code (see Fig.1 of Kravtsov, Klypin, & Hoffman 2001).

### 3. Results

For each simulation, clusters were identified in the refined subvolume and their virial radii ( $r_{vir}$ ) determined as the radius at which the mean enclosed density was  $\Delta_c$  times the critical density (at  $z = 0$ ,  $\Delta_c \sim 101$  for  $\Lambda$ CDM and 178 for SCDM; e.g., Bryan & Norman 1998). Projected gas density, X-ray surface brightness, and emission-weighted gas

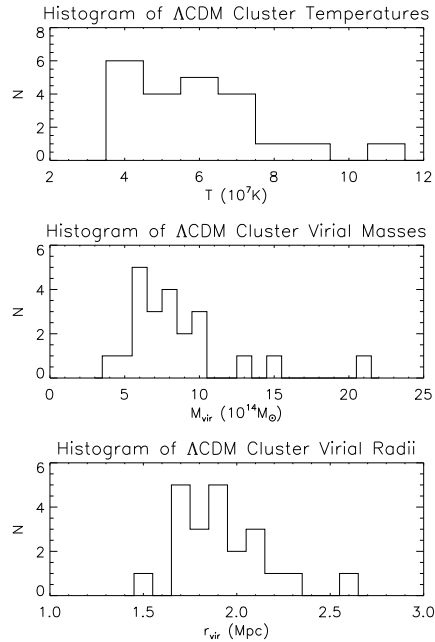


Fig. 1.— Histograms of the temperature, mass and virial radius distributions for the  $\Lambda$ CDM sample of simulated clusters.

temperature images ( $5 h^{-1}$  Mpc on a side) were constructed for each cluster assuming a Raymond-Smith spectrum with metallicity 0.3 solar in the (1.5-11.0) keV bandpass used in the analysis of M98. 2D radial temperature profiles (centered on the X-ray peak) were determined from the temperature images and a global temperature ( $T_x$ ) calculated by summing the emission-weighted temperature within  $1.0 h^{-1}$  Mpc. This procedure was intended to duplicate, as closely as possible, that of M98.

The distribution of cluster temperatures ( $T_x$ ), virial masses ( $M_{vir}$ ), and virial radii ( $r_{vir}$ ) in the  $\Lambda$ CDM sample are shown in Fig. 1. The complex, non-isothermal structure of the clusters is shown in the thumbnail images in Fig. 2. Although complicated, a number of patterns can be discerned: the core of the cluster is generally hotter than the outskirts; low-temperature “holes” correspond to

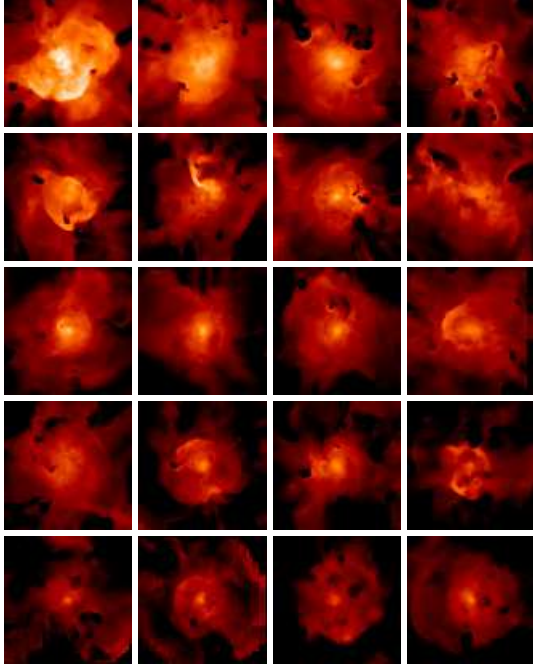


Fig. 2.— Projected emission-weighted temperature maps of the  $\Lambda$ CDM clusters at  $z = 0$ . Each image is  $5 \text{ h}^{-1} \text{ Mpc}$  on a side. Clusters are ordered from most massive (top left) to least massive (bottom right).

infalling groups with lower masses and hence, lower temperatures. In addition, a few clusters show strong shocks due to recent major mergers, but these are generally not spherically symmetric and tend to be of order a Mpc from the core and so might be difficult to detect observationally. The evolution of the temperature structure and the significant differences between SCDM and  $\Lambda$ CDM clusters at  $z = 0.5$  will be discussed in a forthcoming paper (Loken et al. 2002).

The key result of this current paper concerns the 2D temperature profiles shown in Figs. 3 and 4. A given cluster’s temperature profile is normalized by its global temperature ( $T_x$ ) and the radius is scaled by the cluster’s virial radius. Note that the resulting profiles are remarkably similar even when comparing

$\Lambda$ CDM and SCDM clusters. In addition, the majority of the profiles fall within the band drawn by M98 (reproduced in Figs. 3 and 4) to encompass the majority of their data points and error bars.

Fig. 4 is a “tidied” version of Fig. 3 which includes only those clusters whose X-ray appearance is fairly regular and symmetric. This is exactly the same selection cut imposed by M98 and others searching for a general temperature profile. However, even the excluded profiles are, for the most part, not dramatically different in general appearance. The discarded profiles generally have strong bumps or wiggles at the radius corresponding to a merging subcluster. 13 of 22  $\Lambda$ CDM cluster profiles are kept in Fig. 4 (similarly, M98 find that 17 of their 33 clusters are symmetric). However, only 3 of 10 SCDM cluster are sufficiently regular; presumably this reflects the fact that clusters are still forming at  $z = 0$  in an SCDM universe.

We find that the temperature profiles in Fig. 4 can be well fit with an expression of the form:  $T = T_o [1 + r/a_x]^{-\delta}$ , where  $T_o = 1.33$ ,  $a_x = r_{vir}/1.5$ , and  $\delta = 1.6$  on the radial range  $(0.04 - 1.0) r_{vir}$ . M98 chose instead to fit their temperature profiles with a polytropic equation of state:  $T = T_o [1 + (r/a_x)^2]^{-3\beta(\gamma-1)/2}$ . Using this form on the same radial range as M98,  $(0.09 - 0.55) r_{vir}$ , we find  $T_o = 1.15$ ,  $a_x = r_{vir}/7.2$ , and  $\gamma = 1.26$  (assuming  $\beta = 2/3$ ). M98 found a very similar fit:  $\gamma = 1.24_{-0.12}^{+0.20}$  and  $a_x = r_{vir}/11$ . We note, however, that the shape of the fit changes when the fitted range is extended to  $(0.04 - 1.0) r_{vir}$  in which case:  $T_o = 1.17$ ,  $a_x = r_{vir}/5$  and  $\gamma = 1.39$ . This sensitivity to the choice of fitting range appears to be due to the fact that the scatter in the data decreases for  $r > \sim 0.6 r_{vir}$  and suggests that observations must extend to near the virial radius in order to converge on the true, universal temperature profile.

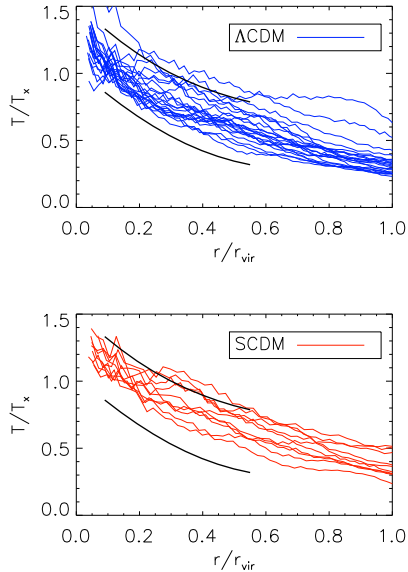


Fig. 3.— Temperature profiles for all the clusters in our  $\Lambda$ CDM (top) and SCDM (bottom) samples. Temperatures and radii are scaled in terms of the cluster’s global temperature and virial radius, respectively. The heavy, black lines are reproduced from Fig. 7 of M98 and enclose most of their data points and error bars.

Though the two forms for the temperature profile both yield acceptable fits, we prefer the first form for two reasons. First, the key difference between the two fits is that the polytropic form turns over and begins to level-off at small radii while the first one continues to rise (just as in Fig. 4). If the fits are extended within  $r = 0.09 r_{vir}$ , then the polytropic form yields an increasingly poor fit. It is difficult to draw any strong conclusions, however, because this is exactly the region within which non-adiabatic effects would become important and, as well, our limiting resolution is  $\sim 0.01 r_{vir}$  for a typical cluster.

The second argument against the polytropic form is the fact that it is not well-motivated physically. In fact, it can be de-

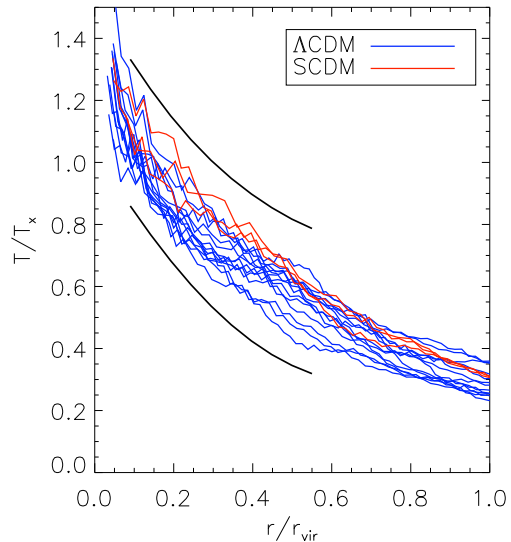


Fig. 4.— Temperature profiles for the symmetric clusters in our  $\Lambda$ CDM (blue) and SCDM (red) samples. Scaling and the observational bounds from M98 are as in Fig. 3.

rived by assuming that the gas is: *isothermal*, follows a  $\beta$ -model for the X-ray surface brightness, and obeys the *polytropic* equation of state,  $T = T_o \rho^{\gamma-1}$ . Clearly, this is an inconsistent derivation. Moreover, the assumption of a polytropic equation of state amounts to assuming that the gas is isentropic which clearly contradicts the outwardly rising entropy profiles which we and others find from simulations (e.g., Frenk et al. 1999).

Recently, De Grandi & Molendi (2002) have analyzed *BeppoSAX* data for a sample of 21 clusters with and without cooling flows. They concluded that non-cooling flow cluster temperature profiles are flat in the innermost regions ( $r < 0.2 r_{vir}$ ) and that the profiles of both types of clusters decline rapidly with radius outside  $r \sim 0.2 r_{vir}$ . Their mean data points for the two types of clusters are shown in Fig 5 along with profiles for two of our clusters which are discussed in §3.1. Again, the

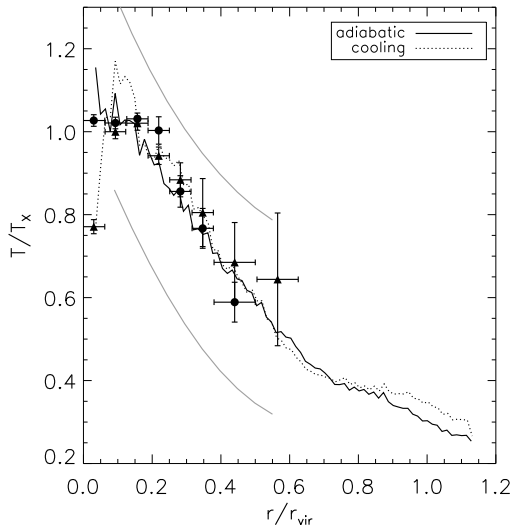


Fig. 5.— Mean temperature profiles (with  $1\text{-}\sigma$  errors) for a sample of 11 cooling flow clusters (filled triangles) and 10 non-cooling flow clusters (filled circles) observed by *BeppoSAX* (De Grandi & Molendi 2002) along with our numerical results for a particular cluster simulated with and without radiative cooling. The grey bands represent the M98 observational bounds as in Fig. 3.

shape and normalization of the observational profiles agree well with the simulations though the flat innermost region may signal the need for some additional physics in the simulations (e.g. De Grandi & Molendi 2002).

### 3.1. Role of Additional Physics

The present adiabatic simulations are the first step in a planned series of simulations which will incorporate non-adiabatic physical effects. Thus they form a baseline sample for evaluating the significance of additional physics. Though potentially important processes like cooling and galaxy feedback are not included in the simulations for the adiabatic cluster catalog, we would expect any effects to be strongly limited to the cluster core and

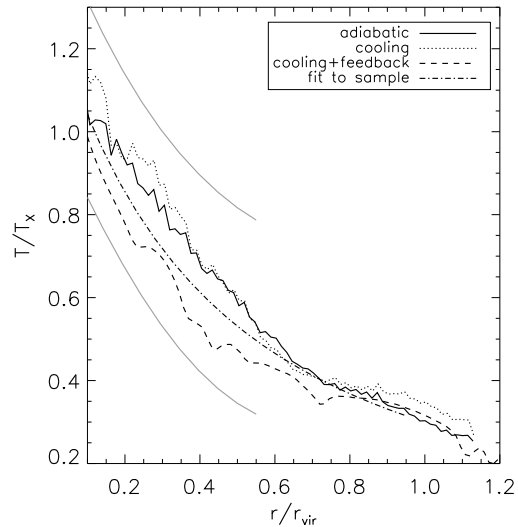


Fig. 6.— Temperature profiles for a cluster from our adiabatic sample (solid line) and the same cluster rerun to include radiative cooling (dotted line). Our fit to the entire sample of symmetric clusters is shown as the dash-dot line. Also shown is the “Santa Barbara” cluster from a simulation incorporating cooling and supernovae feedback. See text for more details. The grey bands are again reproduced from Fig. 7 of M98 and enclose most of their data points and error bars.

to have very little effect in the outer regions. These expectations now appear justified by our most recent non-adiabatic simulations.

Two of the clusters in our sample have been re-run with identical parameters and resolution in order to include the effects of radiative cooling (Motl et al. 2002). These new runs are compared with the adiabatic simulations in Fig. 6. The temperature profiles of the cooling clusters are scaled as in the adiabatic case except that we omit the inner core ( $r < 0.1 r_{vir}$ ) when calculating the global temperature. In addition, one of us (MLN) has recently performed a higher resolution ( $7.8h^{-1}\text{kpc}$ ) simulation including both radiative cooling, and

Type II supernovae feedback. This cluster, which has the same initial parameters as the Santa Barbara comparison cluster (Frenk et al. 1999) is also included on the figure for comparison. We caution that this is just a first simulation and hence the full parameter space of star formation and feedback parameters has not been explored.

Note that, as expected, the temperature profile of the cooling cluster is virtually indistinguishable from that of the adiabatic cluster outside of the cool core ( $r > 0.1 r_{vir}$ ). This strongly suggests that our conclusions about declining cluster temperature profiles are not the result of neglecting radiative cooling. Perhaps even more interesting is the higher-resolution simulation which incorporates both cooling and feedback. Again, the shape of the corresponding temperature profile is remarkably similar to the other cases. Fig. 6 makes clear that the non-adiabatic profiles also fit well within the observational bounds determined by M98

Electron thermal conduction, which is not included in our simulations, would have to be a significant fraction of its Spitzer value in order to erase temperature gradients on the scale we observe. The suppression of thermal conduction by tangled cluster magnetic fields is an open area of research which has, as yet, reached no firm conclusion (Chandran & Cowley, 1998; Malyskin & Kulsrud, 2001).

#### 4. Discussion

We have used our volume-limited catalogs of numerically-simulated clusters to demonstrate that both  $\Lambda$ CDM and SCDM clusters follow a universal cluster temperature profile with  $T/T_o = 1.3[1 + 1.5r/r_{vir}]^{-1.6}$ . This temperature profile agrees very well with the observationally-determined profile of M98 and the more recent *BeppoSAX* data of DeGrandi & Molendi (2002) (Fig. 5). Our simulations

also reveal a wealth of extremely complex and non-isothermal temperature structure (Fig. 2) which current X-ray telescopes may be able to probe. Interestingly, our preliminary analysis suggests that the large-scale cluster temperature structure (particularly for  $z > 0$ ) is a potential discriminator of cosmological model.

Our current adiabatic catalogs of clusters were intended to serve as a well-defined baseline sample for statistical and individual comparison with both observed clusters and with future simulations that include additional physical effects. Remarkably, our initial simulations of clusters with more realistic physics (radiative cooling and galaxy feedback) give rise to temperature profiles (Fig. 6) that agree well with our adiabatic profile and suggest that this truly is a universal cluster temperature profile.

#### Acknowledgements

This work has been partially supported by NASA grant NAG5-7404 and NSF grant AST-9803137. G.L.B. is supported by NASA through Hubble Fellowship grant HF-01104.01-98A from the Space Telescope Science Institute, which is operated under NASA contract NAS6-26555. The simulations were carried out on the SGI/Cray Origin 2000 at the National Center for Supercomputing Application, University of Illinois Urbana-Champaign.

#### REFERENCES

- Berger, M.J. & Collela, P. 1989, *J. Comp. Phys.*, 82, 64
- Bryan, G.L. 1999, *Computing in Science and Engineering*, 1:2, 46
- Bryan, G.L., & Norman, M.L. 1998, *ApJ*, 495, 80
- Chandran, B. & Cowley, S. 1998. *Phys. Rev. Letters*, 80, 3077.
- De Grandi, S., & Molendi, S. 2002, *ApJ*, 567,

163.

- Frenk, C.S. et al. 1999, ApJ, 525, 554
- Irwin, J.A. & Bregman, J.N. 2000, ApJ, 538, 543
- Irwin, J.A., Bregman, J.N., & Evrard, A.E. 1999, ApJ, 519, 518
- Kravtsov, A.V., Klypin, A., & Hoffman, Y. 2001, astro-ph/0109077
- Lin, W., Norman, M.L., & Bryan, G.L. 2001, submitted to ApJ
- Malyshkin, L. & Kulsrud, R. 2001. Ap. J., 549, 402.
- Markevitch, M., Forman, W.R., Sarazin, C.L., & Vikhlinin, A. 1998, ApJ, 503, 77 (M98)
- Metzler, C.A., White, M., Norman, M., & Loken, C. 1999, ApJ, 520, L9
- Metzler, C.A., White, M., & Loken, C. 2001, ApJ, 547, 560
- Motl, P.M., Burns, J.O., Loken, C., Norman, M.L., & Bryan, G. 2002, *in preparation*
- Norman, M.L. & Bryan, G.L. 1999, in Numerical Astrophysics, eds. Miyama, S.M., & Hanawa, T., Kluwer Academic, p. 19
- Norman, M., Daues, G., Nelson, E., Loken, C., Burns, J., Bryan, G. & Klypin, A. 1999, Large Scale Structure in the X-ray Universe, Proceedings of the 20-22 September 1999 Workshop, Santorini, Greece, eds. Plionis, M. & Georgantopoulos, I., Atlantis-science, Paris, France, p.395
- Stone, J.M., & Norman, M.L. 1992, ApJS, 80, 753
- White, D.A., 2000, MNRAS, 312, 663